Catalysis Science & Technology

PAPER

View Article Online
View Journal | View Issue

Check for updates

Cite this: *Catal. Sci. Technol.*, 2018, **8**, 2686

# Structure–function relationship during $CO_2$ methanation over $Rh/Al_2O_3$ and $Rh/SiO_2$ catalysts under atmospheric pressure conditions†

Natalia M. Martin, *[a] Felix Hemmingsson,[a] Xueting Wang,[a] Lindsay R. Merte,[b] Uta Hejral,[c] Johan Gustafson,[c] Magnus Skoglundh,[a] Debora Motta Meira,[d] Ann-Christin Dippel,[e] Olof Gutowski,[e] Matthias Bauer[f] and Per-Anders Carlsson[a]

Received 13th March 2018,
Accepted 20th April 2018

DOI: 10.1039/c8cy00516h

rsc.li/catalysis

The effect of the support material and chemical state of Rh in $Rh/A_2O_3$ and $Rh/SiO_2$ model catalysts during $CO_2$ hydrogenation were studied by a combined array of *in situ* characterisation techniques including diffuse reflectance infrared Fourier transform spectroscopy, energy-dispersive X-ray absorption spectroscopy and high-energy X-ray diffraction at 250–350 °C and atmospheric pressure. $CO_2$ methanation proceeds *via* intermediate formation of adsorbed CO species on metallic Rh, likely followed by their hydrogenation to methane. The linearly-bonded CO species is suggested to be a more active precursor in the hydrogenation compared to the bridge-bonded species, which seems to be related to particle size effects: for larger particles mainly the formation of inactive bridge-bonded CO species takes place. Further, analysis of the chemical state of Rh under the reaction conditions reveal a minor formation of $RhO_x$ from dissociation of $CO_2$, which is a consequence of the increased activity observed over the $Rh/Al_2O_3$ catalyst.

Open Access Article. Published on 23 April 2018. Downloaded on 2/20/2026 5:34:00 PM.
This article is licensed under a Creative Commons Attribution-NonCommercial 3.0 Unported Licence.

## 1 Introduction

Utilisation of $CO_2$ as a reactant for formation of valuable compounds such as hydrocarbons, oxygenates and even carbon monoxide may play an important role in the transition towards a sustainable energy system. Production of methane through $CO_2$ hydrogenation (Sabatier reaction) is a promising route for $CO_2$ utilization:

$$CO_2 + 4H_2 \rightleftharpoons CH_4 + 2H_2O,\ \Delta H_{298} = -165\ \text{kJ mol}^{-1} \quad (1)$$

In addition, this reaction is interesting due to its application in manned space colonisation on Mars or its use in reclaiming oxygen in the International Space Station, where the oxygen resource from $CO_2$ can be transformed into methane and water for fuel and astronaut life-support systems.[1,2]

Catalytic materials that facilitate $CO_2$ hydrogenation must be able to bind and activate $CO_2$ for reaction with dissociated hydrogen. Ni-Based catalysts have been widely investigated for industrial purposes of methane production due to their low cost and ease of availability. Ni catalysts, however, may be deactivated even at low temperatures due to sintering of Ni particles, formation of mobile Ni sub-carbonyls, or carbon deposition.[3,4] Therefore several other transition metals have been investigated for the methanation of $CO_2$ (Ru, Rh, Pd, Co, Fe, Cu, Pt, Mg, Zn, Zr, Ir, Cu, Ag, W, Mo, and Mn) (see ref. 5, 12 and 13 and references therein). Among the noble metals, Ru and Rh on various supports have been shown to be very effective catalysts for the hydrogenation of $CO_2$ and the most selective toward methane.[6–8] Rh is one of the most investigated metals for the $CO_2$ methanation reaction. It has been reported that the support has a marked influence on the specific activity of Rh. An effective support not only provides a high surface area for the metal dispersion but it can also modify the catalytic properties of the metal nanoparticles through the so-called strong metal–support interaction (SMSI) effect.[9]

As pointed out by Puigdollers *et al.*,[10] when used in catalysts, the difference between the nonreducible and reducible oxides is of fundamental importance for their chemical reactivity. Mostly reducible oxides have been reported to have a

[a] *Competence Centre for Catalysis, Department of Chemistry and Chemical Engineering, Chalmers University of Technology, Göteborg, 412 96, Sweden. E-mail: Natalia.Martin@chalmers.se; Fax: +46 31 160062; Tel: +46 31 772 29 04*
[b] *Division of Chemical Physics, Department of Physics, Chalmers University of Technology, Göteborg, 412 96, Sweden*
[c] *Division of Synchrotron Radiation Research, Lund University, 22100 Lund, Sweden*
[d] *European Synchrotron Radiation Facility (ESRF), 38043 Grenoble, France*
[e] *Deutsches Elektronen-Synchrotron (DESY), 22607 Hamburg, Germany*
[f] *Department of Chemistry, Paderborn University, 33098 Paderborn, Germany*
† Electronic supplementary information (ESI) available: Fig. S1 and S2. See DOI: 10.1039/c8cy00516h


This journal is © The Royal Society of Chemistry 2018

Open Access Article. Published on 23 April 2018. Downloaded on 2/20/2026 5:34:00 PM.
This article is licensed under a Creative Commons Attribution-NonCommercial 3.0 Unported Licence.

SMSI effect. In their previous work on $CO_2$ methanation on supported Rh catalysts, Solymosi *et al.*[7] showed that among the investigated supports ($Al_2O_3$, $SiO_2$, MgO and $TiO_2$), the most effective one was $TiO_2$ and the least effective one was $SiO_2$. The effect of the support was attributed to different extents of electronic interaction between Rh and the support, influencing the bonding and the reactivity of the chemisorbed species. Although several papers have been published on the subject during the past decades, no general consensus exists on the operating reaction mechanism and on the active phase of the catalyst.[12,13]

Recently, we have studied different systems consisting of metals (Pd, Rh and Ni) supported on both reducible ($CeO_2$) and nonreducible ($Al_2O_3$ and $SiO_2$) oxides for the activation of $CO_2$ and its reaction with $H_2$ under atmospheric pressure conditions and at relatively low temperatures (250–350 °C).[11] Interestingly, the results showed that Rh supported on both alumina and ceria exhibits high activity in the hydrogenation of $CO_2$ for methane production and the catalysts supported on $SiO_2$ have negligible activity. Therefore, a clear distinction between the reactivity of catalysts supported on reducible *vs.* nonreducible oxides could not be made based on the kinetic data. The selectivity toward $CH_4$ formation was higher for the alumina supported catalysts compared to the ceria supported ones at temperatures up to 350 °C. The kinetic analysis also indicated that on $Rh/CeO_2$ small amounts of CO are formed above 250 °C, while $Rh/Al_2O_3$ shows full selectivity towards methane up to 350 °C. The reason for the high activity over $Rh/Al_2O_3$ was not fully understood. Additional *in situ* infrared spectroscopy (IRS) measurements suggested that the reaction mechanism for the ceria and alumina supported Rh catalysts is different. The likely reaction pathway was found to proceed *via* formation of formates at the Rh–ceria interface or *via* $CO_2$ dissociation and formation of Rh–CO on the $Rh/Al_2O_3$ sample. However, the correlation between the activity/selectivity and surface chemistry of rhodium and the structural properties of both rhodium and ceria or alumina was not accessible with this technique.

In the present report, we give a detailed account of the catalytic behaviour of Rh supported on $Al_2O_3$ and $SiO_2$ under *in situ* conditions. Special attention is paid to the identification of surface species and the effects of alumina and silica supports during the $CO_2$ methanation reaction. The scope of the work is to observe chemical/structural changes of both Rh and the support's phases including chemisorbed species and to relate them to their catalytic behavior. For simplicity, we focus on Rh supported on nonreducible oxides in the present work. *In situ* energy-dispersive X-ray absorption spectroscopy (ED-XAS) and high-energy X-ray diffraction (HE-XRD) have been employed to characterise the dynamic response of supported Rh catalysts when exposed to varying $CO_2$ hydrogenation conditions. The results reveal reversible structural changes of the catalysts under transient operation conditions. The observable changes occur mainly in the Rh phase during the measurements and no significant changes are observed in the alumina or silica phases. The metal–support interaction cannot be excluded for the alumina supported catalyst since a test on the alumina sample showed no measurable methane production under the same reaction conditions. The interaction, however, may be considerably lower as in the case of reducible oxides.[7] The complementary Fourier transform infrared (FTIR) spectroscopy results during the methanation reaction reveal the intermediate surface species formed on the Rh supported catalysts. Differences are observed for $Rh/Al_2O_3$ and $Rh/SiO_2$ and the enhanced activity over Rh/alumina is related to the formation of adsorbed CO species linearly bonded to Rh as well as some $RhO_x$ species resulting from the dissociation of $CO_2$.

The theoretical metal loading is expected to be very close to the actual loading as previously reported for incipient wetness impregnation.[16]

# 2 Experimental section

## 2.1 Catalyst preparation and *ex situ* characterization

The catalysts were prepared by incipient wetness impregnation using powder samples of alumina (Puralox SBa200, Sasol) and silica (Kromasil Silica KR-300-10, Akzo Nobel Eka Chemicals). The powder samples were calcined in air at 600 °C for 2 h starting from room temperature with a heating rate of 5° $min^{-1}$ to remove carbonaceous impurities and stabilise the structure of the support materials. Precursor solutions of rhodium were prepared by dissolving $Rh(NO_3)_3 \times 2H_2O$ (Alfa Aesar) salt in Milli-Q water (18 MΩ cm). To increase the solubility of the rhodium salt, 25 droplets of 70% $HNO_3$ were added. A specific amount of precursor solution to obtain 3 wt% of the metal was added to 3 g of each support. The impregnated alumina and silica samples were instantly frozen in liquid nitrogen, freeze-dried for 24 h and finally calcined in air at 550 °C for 1 h.

The specific surface area of the catalysts was determined by nitrogen sorption at 77 K (Micrometrics Tristar 3000) using the Brunauer–Emmett–Teller (BET) method.[14] The samples were dried under vacuum at 230 °C for 3 h prior to the measurements. The results are summarized in Table 1.

## 2.2 *In situ* measurements

**2.2.1 Energy-dispersive X-ray absorption spectroscopy.** Energy-dispersive (ED) transmission XAS measurements were performed in time-resolved *in situ* mode with synchronous mass spectrometry (MS), see below, at beamline ID24 at the European Synchrotron Radiation Facility (ESRF) in Grenoble, France.[15] The measurements were performed using a Si[311] polychromator in a Laue configuration and a FreLoN detector to monitor the Rh K-edge at 23 220 eV. The experimental setup included a specially designed reaction cell developed at ID24 to meet established practice on simultaneous ED-XAS and diffuse reflectance infrared Fourier transform spectroscopy (DRIFTS) during transient feeding of reactants. The cell has a small reactor volume in which a sample cup with a diameter of 5 mm and a depth of 2.5 mm loaded with about 40 mg of the powder sample is positioned. The gas composition

Open Access Article. Published on 23 April 2018. Downloaded on 2/20/2026 5:34:00 PM.
This article is licensed under a Creative Commons Attribution-NonCommercial 3.0 Unported Licence.

**Table 1** Metal loading, calcination temperature and specific surface area of the catalyst samples used in this study. The catalytic performance as reported in ref. 11 is also included for comparison. The $Rh/Al_2O_3$ catalyst has been reported to have ~100% selectivity to methane formation from $CO_2$ hydrogenation. The theoretical metal loading is expected to be very close to the actual loading as previously reported for incipient wetness impregnation[16]

| Sample | Rh loading (wt%) | Calcination temperature (°C) | Specific surface area ($m^2\ g^{-1}$) | $CO_2$ conversion[11] (350 °C) |
|---|---|---|---|---|
| $Rh/SiO_2$ | 3.0 | 550 | 310 | ~10% |
| $Rh/Al_2O_3$ | 3.0 | 550 | 180 | ~40% |

was controlled by Bronkhorst mass flow controllers and introduced to the cell *via* air actuated high-speed gas valves (Valco, VICI), all in all facilitating rapid gas composition changes over the catalyst sample.

The XAS measurements included both the X-ray absorption near-edge structure (XANES) and extended X-ray absorption fine structure (EXAFS) regions. Energy calibration was performed using a Rh metal foil. After energy calibration the XANES spectra were normalized using the Athena software.[17] The XAS data were further processed and analysed using Athena and Larch software.[18] Fourier transformation of the $k^2$-weighted EXAFS data to the $R$ space was done between $k$ = 3 and $k$ = 10 $Å^{-1}$.

Oxidation and reduction measurements were performed *in situ* at 350, 300 and 250 °C, respectively, with alternating pulses of 2 vol% $O_2$ and 2 vol% $H_2$ (4 min long pulses) by measuring the Rh K-edge. The pulses were repeated 6 times to give a total duration of the experiment of 48 min. The introduction of the first $O_2$ pulse triggered the recording of the XAS spectra. He was used as a carrier gas, and the total gas flow was kept constant at 75 mL $min^{-1}$.

The methanation reaction was performed under transient operation conditions by introducing $H_2$ pulses (2 vol%) to an otherwise constant flow of $CO_2$ (0.5 vol%) at 350, 300 and 250 °C, respectively. The pulses were 10 min long and were repeated 5 times to give a total duration of the experiment of 100 min. Prior to the reaction the catalysts had been reduced in $H_2$ for 10 min at the corresponding temperature at which the reaction was performed. For both the oxidation/reduction and $CO_2$ methanation measurements, the spectra were recorded with a time resolution of 0.87 seconds.

**2.2.2 High-energy X-ray diffraction.** The crystal structure of the samples during the methanation reaction was studied in time-resolved *in situ* mode by high-energy XRD in the second experimental hutch (EH2) of the P07 beamline at PETRA III at Deutsches Elektronen-Synchrotron (DESY) in Hamburg, Germany.[19] A photon energy of 85 keV was employed for the measurements and the incoming beam focused to a size of 2 × 30 $\mu m^2$ was directed at the surface. A large two-dimensional 400 × 400 $mm^2$ Perkin Elmer XRD1621 detector with 200 × 200 $\mu m^2$ pixel size and adapted for X-rays with energy higher than 20 keV was used for the recording of diffraction patterns.

Similar to the ED-XAS experiments, the gas feed composition was controlled by mass flow controllers and introduced to the cell *via* air actuated high-speed gas valves. The methanation reaction was performed under transient operation conditions by introducing $H_2$ pulses (2 vol%) to an otherwise constant flow of $CO_2$ (0.5 vol%) at 350, 300 and 250 °C, respectively. The pulses were 10 min long and were repeated 5 times to give a total duration of the experiment of 100 min. The time resolution of the measurements was 0.5 seconds. For these measurements, a specially designed reaction cell was employed which is described in detail elsewhere.[20]

**2.2.3 *In situ* FTIR spectroscopy.** The *in situ* FTIR spectroscopy experiments were performed in diffusive reflectance (DRIFT) mode with a BRUKER Vertex 70 spectrometer equipped with a nitrogen cooled MCT detector and a high-temperature stainless steel reaction cell (Harrick Praying Mantis™ High Temperature Reaction Chamber) with KBr windows. The temperature of the sample holder was measured using a thermocouple (type K) and controlled by a PID regulator (Eurotherm). Feed gases were introduced into the reaction cell *via* individual mass flow controllers, providing a total flow of 100 ml $min^{-1}$ in all experiments. Prior to the experiment the samples were pre-treated at 350 °C with 5 vol% $O_2$ in Ar for 10 min and 0.8 vol% $H_2$ in Ar for 10 min and then cooled in Ar to the desired temperature where a background spectrum was collected. The experiment was performed by introducing a flow of 0.2 vol% $CO_2$ and 0.8 vol% $H_2$ to the reaction cell and a spectrum was measured after 20 min in the reaction mixture at 350 °C. The region between 790–3800 $cm^{-1}$ was investigated with a spectral resolution of 8 $cm^{-1}$.

# 3 Results and discussion

### 3.1 *In situ* characterization of the redox behavior

When the methanation reaction is performed, the catalyst is exposed to a reductant ($H_2$) and an oxidant ($CO_2$). Since the catalyst may change its oxidation state during this reaction, especially under transient operation conditions, it is important to elucidate how the catalyst behaves under oxidation or reduction conditions. Transient oxidation and reduction of the Rh-based catalysts was studied by *in situ* ED-XAS. Fig. 1 shows the evolution of the XAFS spectra for the $Rh/Al_2O_3$ sample at 350 °C during the oxidation–reduction cycling experiment in either 2 vol% $O_2$ or 2 vol% $H_2$. The experiment starts with a 4 min oxidation pulse. The left panel (a) shows the XAS spectra recorded at the end of the oxidation and reduction periods, while the right panel shows the recorded XAS spectra as a function of time (b) together with the white line intensity during the experiment (c). The strong peak above the edge, *i.e.* the white line, corresponds to the 1s–4d

 This journal is © The Royal Society of Chemistry 2018

Open Access Article. Published on 23 April 2018. Downloaded on 2/20/2026 5:34:00 PM.
This article is licensed under a Creative Commons Attribution-NonCommercial 3.0 Unported Licence.

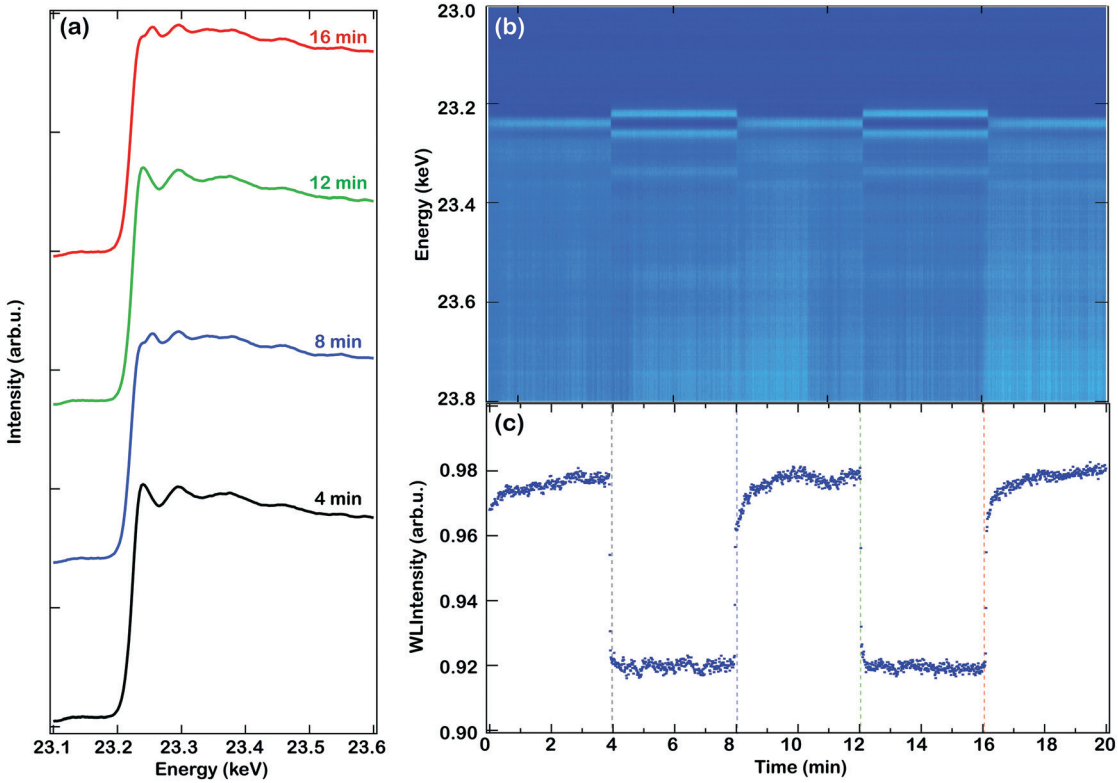


**Fig. 1** XAS spectra of Rh K-edge recorded during consecutive 4 min oxidising (2 vol% $O_2$) and reducing (2 vol% $H_2$) periods over $Rh/Al_2O_3$ at 350 °C. (a) XAS spectra recorded at the end of the oxidising and reducing periods. (b) Color-coded intensities of XAS spectra (blue: low intensity; red: high intensity) and (c) the XAS white line intensity at 23 240 eV. The time dependent spectra in (b) are presented as difference spectra implying that a couple of initial spectra have been subtracted from all spectra in order to facilitate the observation of the major changes occurring during the measurements.

transition at the Rh K-edge and is directly related to the density of vacant d-orbital states. Therefore we have used the white line intensity to monitor the oxidation of Rh. However, other effects, such as that of particle size, can also contribute to the intensity of the white line.[21,22] As observed in the figure, there is a sharp increase in the white line intensity during the $O_2$ pulse which increases further during the first minute of the oxidation cycle, later reaching a maximum intensity, and there is a fast decrease in the white line intensity when the $O_2$ supply is switched off and $H_2$ is introduced to the feed. This indicates a fast oxidation/reduction kinetics of the Rh nanoparticles and since the white line intensity seems to be stable under both the oxidation and reduction conditions a change in the particle size is not likely to occur.

The XAS spectra in Fig. 1(a) are clearly different when they are recorded at the end of an oxidising period compared to the end of a reducing period, whereas the spectra recorded at different oxidising or reducing periods are very similar to one another. Similar results are obtained for the $Rh/SiO_2$ sample. Fig. 2 displays the Rh K-edge XANES and EXAFS spectra of the $Rh/Al_2O_3$ and $Rh/SiO_2$ catalysts during the end of the oxidising and reducing periods at 250, 300 and 350 °C, respectively. The XANES spectra (left panels) show a decreased white line intensity for the $H_2$ treated samples, indicating that Rh is in a reduced state, while the white line intensity increases during the $O_2$ treatment, indicating the oxidation of Rh. The left panels show the XANES spectra recorded from the reduced or oxidised samples at different temperatures. A similar behavior to that of $Rh/Al_2O_3$ is observed for the $Rh/SiO_2$ sample, *i.e.* a decreased white line intensity under the reducing conditions and an increased intensity under oxidising conditions. For the $Rh/SiO_2$ sample, oxidising treatment at 350 °C results in a higher increase of the white line intensity compared to the oxidising treatment at lower temperatures, suggesting a thicker oxide formation or a change in the particle size. By comparing the XAS spectra of the alumina and silica supported Rh catalysts it can be observed that the spectra for $Rh/SiO_2$ in general show a higher intensity of the white line and of the EXAFS oscillations. This indicates an increased number of neighboring atoms, in line with our recent XRD results for the as-prepared catalyst which suggested larger particles of Rh oxide for the silica supported sample.[11]

To gain more information about the local structure surrounding the Rh atoms, a qualitative EXAFS analysis was performed. The associated Fourier transforms are shown on the right panels in Fig. 2, where $R$ represents the radial distance from the absorbing atom. As no phase shift correction was applied, the peaks are observed at distances shorter than those of the actual positions.

Open Access Article. Published on 23 April 2018. Downloaded on 2/20/2026 5:34:00 PM.
This article is licensed under a Creative Commons Attribution-NonCommercial 3.0 Unported Licence.

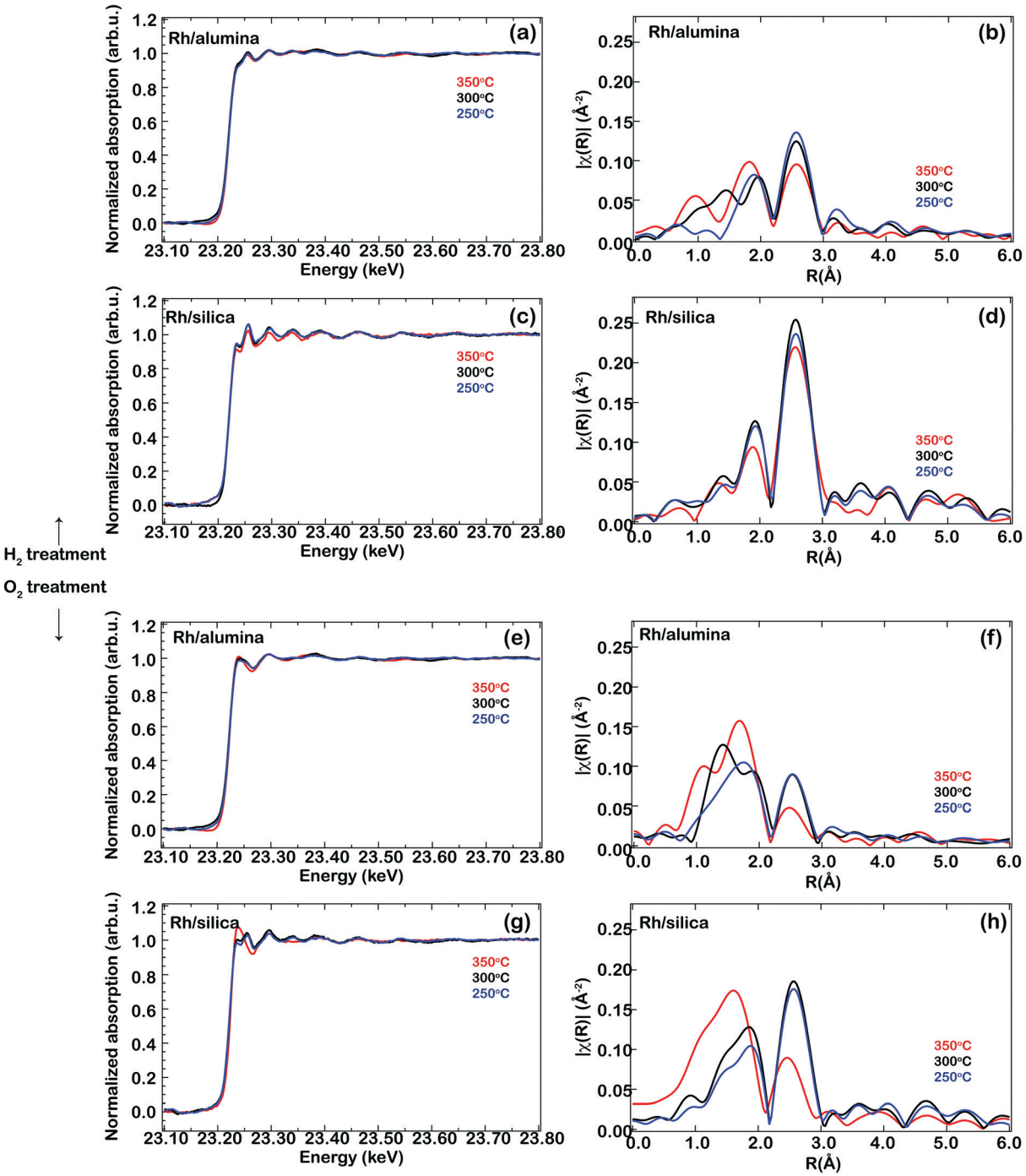


**Fig. 2** Rh K-edge *in situ* XAS spectra (XANES and EXAFS) for the reduced (a–d) and oxidised (e–h) Rh-based catalysts at 350 (red), 300 (black) and 250 °C (blue), respectively.

The EXAFS spectra recorded from the samples exposed to reducing conditions (Fig. 2(b and d)) show the presence of two coordination shells: a peak at a radial distance of 2.57 Å, which is attributed to metal–metal scattering (Rh–Rh bond, first coordination shell) and a low-intensity peak at lower coordination distances, below 2 Å (1.94 Å), attributed to Rh–O scattering from the first shell of $Rh_2O_3$.[23,24,26] The presence of a Rh–O coordination shell during exposure to reducing conditions indicates that the samples contain a fraction of irreducible Rh.

When the samples are exposed to oxidising conditions, the EXAFS spectra show a decrease in intensity of the Rh–Rh scattering peak (~2.5 Å) and an increase of the peak at lower *R*, below 2 Å (due to Rh–O scattering). The weakness of the Rh–O peak intensity at temperatures below 350 °C and the absence of the Rh–O–Rh peak at 2.7 and 3.3 Å as expected for other shells of $Rh_2O_3$ (ref. 23, 24 and 26) suggest that small Rh oxide particles exist on the support materials, and/or an interaction between Rh and O atoms in the support. Contributions from both Rh–O and Rh–Rh scattering under

 This journal is © The Royal Society of Chemistry 2018

Open Access Article. Published on 23 April 2018. Downloaded on 2/20/2026 5:34:00 PM.
This article is licensed under a Creative Commons Attribution-NonCommercial 3.0 Unported Licence.

reducing or oxidising conditions are observed at all temperatures for both samples indicating that, for both samples, Rh is not fully reduced or oxidised under the present experimental conditions. Since XAS is a bulk sensitive technique and the presence of the Rh–Rh coordination shell for both samples indicates that the samples can be envisaged as a metal core with an oxidic outer layer (its thickness depends on the temperature for the oxygen exposure, *i.e.* thicker oxide at 350 °C for both $Rh/Al_2O_3$ and $Rh/SiO_2$).

According to the results presented in Fig. 2, the proportion of reduced Rh after exposure to reducing conditions is higher for $Rh/SiO_2$ than for $Rh/Al_2O_3$. It is known that Rh particles supported on alumina can interact with the surface avoiding reduction of the particles as reported previously by Hwang *et al.*[27] Therefore, the results suggest that there is a higher degree of interaction with the support for the alumina-supported sample as compared to the silica-supported one. However, there are no contributions observed from a Rh–O–Al shell which shall appear at a distance above 2.5 Å ($R \sim 2.5$–3 Å), suggesting that the metal–support interaction is somehow weaker than, for example, in the case of ceria-supported Rh (ref. 23 and 24) or aged alumina-supported Rh (ref. 25 and 26) which have shown such contributions.

### 3.2 *In situ* studies of the $CO_2$ methanation reaction under atmospheric pressure conditions

Structural changes of the Rh and support phases during $CO_2$ hydrogenation over $Rh/Al_2O_3$ and $Rh/SiO_2$ under atmospheric pressure conditions in the temperature range 250–350 °C were monitored in time-resolved *in situ* mode with ED-XAS and HE-XRD and the results are presented below. The activity of the catalysts measured by mass spectrometry showed results comparable to the ones reported on our previous publication[11] and summarized in Table 1 and, for simplicity, we focus here on the structural changes of the Rh and support phases occurring during the $CO_2$ methanation reaction.

**3.2.1 ED-XAS.** To investigate the chemical state and local structure of the Rh atoms in the alumina and silica supported catalysts during the $CO_2$ methanation reaction, XAS data were collected under *in situ* conditions at the Rh K-edge. The live measurements during transient hydrogenation of 0.5 vol% $CO_2$ (1 : 4 ratio of $CO_2$ : $H_2$) at 300 °C are presented in Fig. S1 in the ESI.† The data are presented as difference spectra implying that a couple of initial spectra have been subtracted from all spectra in order to facilitate the observation of the major changes occurring during the measurements. No clear changes are observed in the XAS spectra of the Rh K-edge (nor in the white line intensity) when the catalysts are exposed to $CO_2$ or a $CO_2$ + $H_2$ mixture at 300 °C. However, some differences are observed in the EXAFS analysis. Spectra recorded at the end of the $CO_2$ hydrogenation and $CO_2$ pulses at 350 and 300 °C, including both XANES and EXAFS, are presented in Fig. 3 below.

For the $Rh/Al_2O_3$ sample, the decreased white line intensity of the Rh K-edge XANES spectra in Fig. 3(a) indicates that the state of Rh is predominantly metallic. The Fourier transforms of the Rh K-edge EXAFS spectra of the $Rh/Al_2O_3$ catalyst during methanation reaction at different temperatures are presented in Fig. 3(b). The spectra feature a peak at about 2.5 Å indicative of a Rh–Rh bond. However, an additional peak below 2 Å is observed at all temperatures, indicative of Rh–O bonding, similar to the results obtained under reducing conditions and presented above. The EXAFS analysis of the spectra recorded at 300 °C shows no clear differences between $Rh/Al_2O_3$ exposed to $CO_2$ and $CO_2$ + $H_2$. However, when the measurements were performed at 350 °C, the EXAFS analysis shows a decrease of the Rh–O bond peak intensity during the methanation of $CO_2$ suggesting a

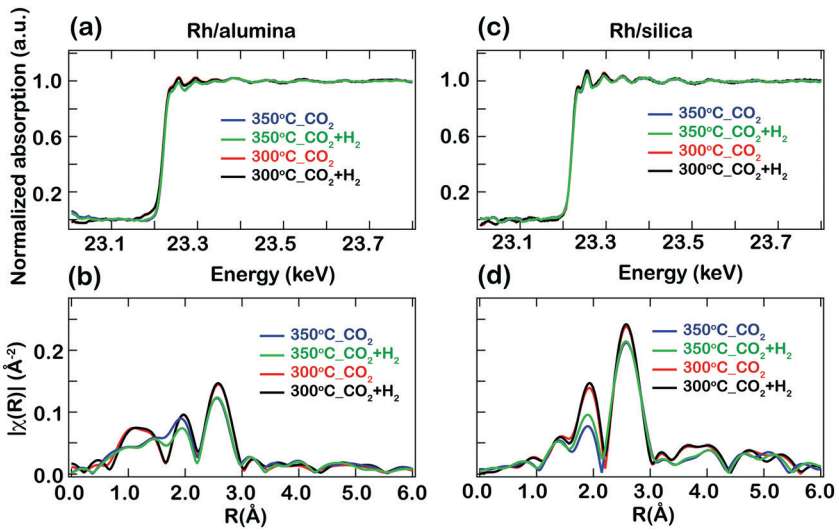


**Fig. 3** Rh K-edge *in situ* XAS spectra (XANES – upper panels and EXAFS – lower panels) for the Rh-based catalysts supported on either alumina (a and b) or silica (c and d) recorded during the transient hydrogenation of $CO_2$. The selected spectra were recorded after the samples had been exposed to pulses of either 2 vol% $H_2$ + 0.5 vol% $CO_2$ or 0.5 vol% $CO_2$ for 10 min at different temperatures.

Open Access Article. Published on 23 April 2018. Downloaded on 2/20/2026 5:34:00 PM.
This article is licensed under a Creative Commons Attribution-NonCommercial 3.0 Unported Licence.

decrease in the oxidation state of Rh as compared to when exposed to $CO_2$. This coincides with the high $CO_2$ conversion and the increased methane selectivity observed for this catalyst under the present experimental conditions. We cannot exclude that some Rh atoms are still bonded to O during the methanation reaction since some Rh–O bond scattering is still visible in the spectra. This is most likely due to some chemisorbed O or from the interaction with the alumina support and its origin will be discussed further below (section 3.2.4). This difference has been observed to be reversible when switching back and forward between the $CO_2$ and $CO_2$ + $H_2$ pulses.

For the $Rh/SiO_2$ sample the XANES data presented in Fig. 3(c) show an overall higher white line intensity of the Rh K-edge, which may indicate an increased oxidation state of the Rh atoms, or larger particles, similar to the results from the oxidising/reducing treatments presented above. The EXAFS analysis shown in Fig. 3(d) shows a strong peak at around 2.5 Å indicative of a Rh–Rh bond at both temperatures and a lower intensity peak just below 2 Å indicative of a Rh–O bond. Thus the larger particle size for the silica supported catalyst is a more plausible explanation for the increased white line intensity. The intensity of the Rh–O peak decreases at higher temperatures, similar to the results obtained during the treatment in a reducing atmosphere. By comparing the EXAFS spectra recorded during the exposure to $CO_2$ + $H_2$ with the spectra recorded during $CO_2$ exposure, even though a slight increase in the Rh–O bond peak intensity is observed during the $CO_2$ methanation at 350 °C, the relative intensity of the Rh–Rh and Rh–O peaks is still higher indicating that Rh is present in a more metallic state in $Rh/SiO_2$ as compared to that in the $Rh/Al_2O_3$ sample.

**3.2.2 HE-XRD.** To obtain further insights into the chemical state of Rh and into any changes the support may undergo during the methanation reaction, transient hydrogenation of $CO_2$ has been investigated under *in situ* conditions by HE-XRD. The result of a time-resolved measurement during periodic variation of the feed gas composition between 2 vol% $H_2$ + 0.5 vol% $CO_2$ and 0.5 vol% $CO_2$ at 350 °C for 10 min over $Rh/Al_2O_3$ is shown in Fig. 4. The cycles of $CO_2$ + $H_2$/$CO_2$ have been repeated 5 times leading to a total duration of the experiment of 100 min. Similar to the XAS results presented above, the data are presented as difference diffractograms to facilitate the observation of the major changes occurring during the pulsed experiments. However, no clear changes could be observed in the XRD patterns between the $CO_2$ or $CO_2$ + $H_2$ pulses during the time-resolved measurements. Selected XRD patterns are shown on the bottom of Fig. 4. The diffraction pattern mainly shows reflections from alumina. A weak broad reflection is observed at $q$ = 2.85 $Å^{-1}$ which is more pronounced during the $CO_2$ methanation (see the inset). A simple analysis employing Bragg's law[31] yields a $d$ spacing for the reflecting planes of $d$ = 2.2 Å at $q$ = 2.85 $Å^{-1}$ and $\lambda$ = 0.155 Å. This value has been compared to tabulated values of $d$ spacings for Rh or Rh oxides available on the ICSD data collection.[32] The tabulated $d$ spacing values of the most intense reflections from Rh and Rh oxides are collected in Table 2 below. By comparing the reported values to the measured value in this study ($d$ = 2.2 Å) we can see that our value lies in between the reported values of Rh and Rh oxides, closer to reflections from metallic Rh. A slight oxidation of Rh or interaction with the support may change the unit cell parameters and therefore lead to a different value of the $d$ spacing which can explain the difference between the tabulated and obtained $d$ spacing values. Therefore we assign the observed reflection to $RhO_x$ scattering. This finding is in agreement with the XAS results which indicated that Rh is not in a pure metallic state during the methanation of $CO_2$, but some Rh–O bonding is likely to coexist with the metallic phase of Rh. This is a strong indication that $CO_2$ dissociates forming adsorbed CO and O.

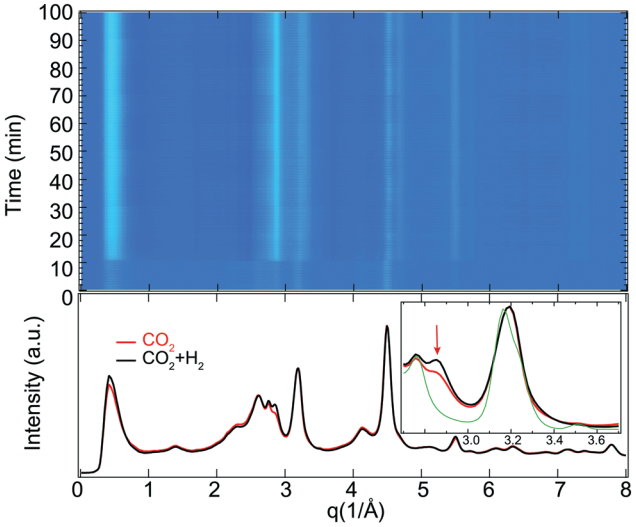


**Fig. 4** Transient hydrogenation of 0.5 vol% $CO_2$ over $Rh/Al_2O_3$ during periodic variation of the feed gas composition between 2 vol% $H_2$ + 0.5 vol% $CO_2$ and 0.5 vol% $CO_2$ at 350 °C for 10 min recorded using HE-XRD. The top panel shows the color coded intensities (blue corresponds to low intensity, red to high intensity) of the XRD patterns in the region 0–8 $Å^{-1}$ *versus* time. The bottom panel shows selected XRD patterns at the end of selected $CO_2$ (red) or $CO_2$ + $H_2$ (black) pulses. The inset indicates a zoom in between 2.7 and 3.7 $Å^{-1}$.

Comparing the analysis of the diffraction pattern recorded during the $CO_2$ pulse to the pattern recorded during the $CO_2$ + $H_2$ pulse it is observed that the $RhO_x$ reflection broadens during the $CO_2$ pulse and is sharper during the methanation reaction. This difference is only observed at 350 °C (see Fig. S2, ESI†) and can be explained by a change in the apparent crystallite size: larger crystallites give sharper reflections. This is in line with the XAS results presented above which

**Table 2** Measured values of the most intense reflections for the Rh and Rh oxides using the ICSD data collection[32]

| Structural formula | Bragg plane | $d$ (Bragg spacing) (Å) | ICSD ref no. |
|---|---|---|---|
| Rh | (111) | 2.07 | #171677 |
| $Rh_2O_3$ | (002) | 2.7 | #41534 |
| $RhO_2$ | (111) | 2.8 | #251565 |


This journal is © The Royal Society of Chemistry 2018

Open Access Article. Published on 23 April 2018. Downloaded on 2/20/2026 5:34:00 PM.
This article is licensed under a Creative Commons Attribution-NonCommercial 3.0 Unported Licence.

indicated a reduced amount of oxidised Rh during the $CO_2$ hydrogenation at 350 °C which is likely due to the increased particle size. However, the discrepancy in the amount of Rh oxide formed during the methanation at 350 °C over the $Rh/Al_2O_3$ sample between the XAS and XRD results may be related to disordered *vs.* well-ordered phases. The $RhO_x$ species resulting from $CO_2$ dissociation in the presence of $H_2$ seem more ordered as compared to the oxide species determined by XAS during the $CO_2$ pulse.

Based on the XRD results it can be concluded that crystalline $RhO_x$ forms during the methanation of $CO_2$ and is likely linked to the increased activity of the $Rh/Al_2O_3$ catalyst. No metallic Rh reflections are observed at any time in the XRD patterns during the $CO_2$ or $CO_2$ + $H_2$ pulses, in contrast to the EXAFS analysis where some Rh–Rh components are visible at all times. XRD classically provides information on structures with long-range order for phase identification and the estimation of apparent crystallite/particle size, and therefore, non-crystalline Rh or very small Rh particles will not be identified by XRD. The formation of some Rh-carbide has been questioned under the present experimental conditions, possibly resulting from the dissociation of adsorbed CO species. However, the *in situ* XAS and XRD measurements do not show any evidence of carbide formation and, therefore, it is likely that its formation does not occur.

**3.2.3 FTIR results.** *In situ* FTIR spectroscopy in diffuse reflectance mode has been employed to study the surface interaction of $CO_2$ and $H_2$ with the Rh catalysts in order to identify the adsorbed species responsible for the catalytic activity. A detailed DRIFTS study of $CO_2$ hydrogenation over $Rh/Al_2O_3$ under transient operation conditions has been presented in our previous publication[11] and, therefore, here we focus our attention on the different surface species formed during the reaction and how these differ depending on the choice of the support.

The DRIFTS results from a steady-state measurement obtained after the $Rh/Al_2O_3$ and $Rh/SiO_2$ catalysts have been exposed to a flow of 0.2 vol% $CO_2$ and 0.8 vol% $H_2$ at 350 °C for 20 min are presented in Fig. 5. The interaction of Rh-based catalysts with a 0.2 vol% $CO_2$ and 0.8 vol% $H_2$ mixture at 350 °C results in the development of bands around 2020 and 1800 $cm^{-1}$, indicating dissociation of $CO_2$ and formation of Rh-bonded carbonyl species. This fact suggests that $CO_2$ hydrogenation proceeds *via* the dissociation of $CO_2$ forming adsorbed CO and O as an intermediate reaction step. Some differences are observed between the two investigated catalysts.

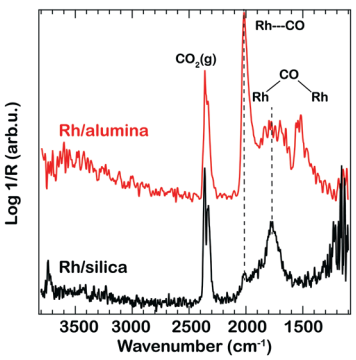


**Fig. 5** IR absorption bands in the wavenumber region 1100–3800 $cm^{-1}$ for the $Rh/Al_2O_3$ (red) and $Rh/SiO_2$ (black) catalysts exposed to 0.2 vol% $CO_2$ and 0.8 vol% $H_2$ at 350 °C for 20 min.

For the $Rh/Al_2O_3$ sample, a strong absorption band centred around 2020 $cm^{-1}$ corresponding to linearly adsorbed CO species on Rh (Rh–CO) appears during $CO_2$ hydrogenation, suggesting $CO_2$ dissociation, in agreement with previous reports on $CO_2$ methanation over $Rh/Al_2O_3$.[28] A broad band around 1780 $cm^{-1}$ is also detected, which is close to the reported values of bridge-bonded CO on Rh ($Rh_2^0$-CO, ~1800 $cm^{-1}$).[33,34] Some additional weaker peaks in the region 1700–1500 $cm^{-1}$ are also visible corresponding to carbonate or formate-like species on the alumina support.

The positions of adsorbed carbonyl bands are shifted to lower vibrational frequencies during the $CO_2$ hydrogenation as compared to reported values for adsorbed carbonyl species. This trend has previously been reported in the literature and can be attributed to the formation of Rh carbonyl hydrides (Rh–CO–H).[6,7,28–30] A reduction of the surface coverage of these species can produce a decrease in CO(ads) dipole–dipole coupling and may also contribute to the observed shift.

For the $Rh/SiO_2$ sample the band associated with bridge-bonded CO on Rh increases in intensity during the $CO_2$ hydrogenation, while the band assigned to linearly adsorbed CO on Rh has a much lower intensity. The preferred adsorption of CO in bridge coordination is likely due to the increased particle size for this sample compared to the alumina supported sample, as previously observed for $Rh/TiO_2$.[35] The adsorption and dissociation of $CO_2$ is enhanced by the presence of $H_2$ since experiments with exposure to $CO_2$ only result in less intense absorption bands (not shown). The decreased content of linearly adsorbed CO species on Rh may be responsible for the low activity observed over this sample, which may indicate that the bridge-bonded CO on Rh only is a spectator species in the $CO_2$ hydrogenation. Generally a decrease of CO adsorbed species is observed for the silica supported catalyst likely due to the larger particles and/or an increased difficulty of the silica supported catalyst to dissociate $CO_2$.

No vibrations from adsorbed $CH_x$ species (2800–3000 $cm^{-1}$) could be seen for $Rh/Al_2O_3$ or $Rh/SiO_2$. Further we do not see the presence of CO species adsorbed on $Rh^+$ sites, which previously has been reported in the case of $CO_2$ hydrogenation over $Rh/Al_2O_3$.[36] Therefore, our combined XAS, XRD and DRIFTS results indicate that the first step in the reaction mechanism for $CO_2$ hydrogenation over supported Rh is dissociative adsorption of $CO_2$ forming adsorbed CO and O. The CO adsorbs on the metallic Rh while some other Rh atoms can interact with the O formed by the dissociation of $CO_2$ forming $RhO_x$ as supported by *in situ* XAS and XRD results.

**3.2.4 Discussion of the active species and the role of the support in the methanation reaction.** In this work,

Open Access Article. Published on 23 April 2018. Downloaded on 2/20/2026 5:34:00 PM.
This article is licensed under a Creative Commons Attribution-NonCommercial 3.0 Unported Licence.

characterization of the chemical state of Rh and the role of nonreducible oxides during $CO_2$ methanation under atmospheric pressure conditions and at relatively low temperatures (below 350 °C) has been performed. The chemical state of Rh is studied by *in situ* ED-XAS and HE-XRD and evolution of the different surface species formed during the reaction is studied by *in situ* DRIFTS and their implications in the mechanism of $CO_2$ methanation is discussed below. The results reveal reversible structural changes of the catalysts under transient operation conditions. Two nonreducible oxides (silica and alumina) have been chosen for comparison since previous kinetic studies revealed different catalytic behaviors during the $CO_2$ methanation reaction.[11] Thus the difference between them shall reveal key intermediates responsible for the catalytic activity.

There are several mechanistic and kinetic studies in the literature on $CO_2$ hydrogenation. However, little effort has been made to characterize the surface structure of the catalysts under the reaction conditions and their relation to the catalytic activity for $CO_2$ methanation. In fact, to our knowledge, there are only a few studies available in the open literature on the characterization of the surface structure and its relation to the catalytic activity for Rh-based catalysts on the $CO_2$ methanation reaction, mostly based on DRIFT spectroscopy. There are some speculations regarding the chemical state of Rh during the methanation reaction, based on *ex situ* studies. Some *ex situ* XPS studies on $Rh/Al_2O_3$ have suggested formation of $Rh^{3+}$ species during the methanation reaction. However, the *in situ* DRIFTS results suggested that the active state of Rh during the reaction is very likely to be $Rh^0$.[28] Further, Karelovic *et al.*[28] reported bridge-bonded CO to be more reactive than linearly-bonded CO at low temperatures (150 and 200 °C).

The present *in situ* XAS and XRD results obtained for the highly active $Rh/Al_2O_3$ provide evidence that Rh is slightly oxidised during the methanation reaction and not fully reduced. Comparing the XAS spectra obtained during the $CO_2$ hydrogenation (Fig. 3) to the spectra obtained during the reduction period (Fig. 2), one can observe that at 350 °C the $Rh/Al_2O_3$ catalyst is more reduced during $CO_2$ hydrogenation as compared to when it is exposed to an $H_2$ treatment. A possible explanation for the increased oxidation during the $H_2$ treatment may be the smaller particle size and therefore there is a stronger interaction with the support which in turn hinders the reduction of the small particles.

Nevertheless, the active state of Rh during the reaction is very likely $Rh^0$. As observed by *in situ* DRIFTS experiments, only $Rh^0$–$(CO)_x$ ($x$ = 0.5, 1) species are detected and the linearly adsorbed CO on Rh is found to be the intermediate species in the reaction. Rh–CO species are proposed to be associated with H forming Rh carbonyl hydride species (Rh–CO–H). CO adsorbed on oxidised Rh, which would appear in the 2090–2135 $cm^{-1}$ region,[37] was not detected in our measurements. It is shown that the linearly-bonded CO species are responsible for the increased activity for $CO_2$ hydrogenation compared to the bridge-bonded species under the investigated reaction conditions. These are related to the particle size effects: for larger particles mainly the formation of inactive bridge-bonded CO species takes place. However, some Rh–O bonds are detected by XAS and are likely due to oxidised Rh from the O atoms from the dissociation of $CO_2$ or from internal layers of the particles (*i.e.*, close to the alumina surface). These results are in agreement with previous reports suggesting the reduced Rh species to play an important role in the reaction mechanism.[36,38]

By comparing the results obtained on a highly active catalyst ($Rh/Al_2O_3$) to the ones obtained on a less active one ($Rh/SiO_2$), it can be concluded that the effect of the support on the methanation reaction for nonreducible oxides provides a high dispersion of the active phase. Some electronic interaction between the Rh and the support, influencing the bonding and the reactivity of the chemisorbed species, cannot be excluded and it is shown that the alumina support interacts with Rh facilitating the adsorption and dissociation of $CO_2$. The results are in agreement with a previous study by Rönsch *et al.* who reported that $CO_2$ conversion can be enhanced by a supporting material that fosters high $CO_2$ coverage (*e.g.*, $Al_2O_3$).[13]

Regarding the reaction mechanism for $CO_2$ methanation, two reaction mechanisms have previously been reported in the literature. The first mechanism involves the adsorption of $CO_2$ on the support and its reaction with H(ads) species formed on the metal which leads to the formate intermediate (COOH) at the metal–support interface. The formates can give rise to CO(ads) species which are subsequently hydrogenated to $CH_4$.[39] The second mechanism involves the direct dissociation of $CO_2$ to CO(ads) and O(ads) on the metal surface, with CO(ads) being subsequently hydrogenated to $CH_4$.[33,36,38,40] In our case the direct dissociation of $CO_2$ seems to be evidenced. We have confirmed experimentally that the first step in the mechanism by which the reaction occurs is dissociative adsorption of $CO_2$ on the surface of the catalyst. On $Rh/Al_2O_3$ $CO_2$ adsorption takes place preferably on the metal–support interface, while $CO_2$ dissociation takes place on the active Rh surface and the O can interact with some other Rh atoms forming $RhO_x$. However, the mechanism by which the hydrogen reacts with the dissociated species is not determined in this work and further experiments are needed to clarify the next steps of the reaction.

# 4 Conclusions

*In situ* ED-XAS and HE-XRD studies on $Rh/Al_2O_3$ during the process of $CO_2$ methanation under atmospheric pressure conditions and at relatively low temperatures (below 350 °C) reveal reversible structural changes of the catalysts under transient operation conditions. Such changes were not observed for the $Rh/SiO_2$ catalyst, which also exhibits lower $CO_2$ conversion. Some of the Rh atoms are found to be in a low oxidation state ($RhO_x$) for the highly active $Rh/Al_2O_3$ during the methanation reaction. The *in situ* DRIFTS results indicate that mainly the linearly- and bridge-bonded CO species are

 This journal is © The Royal Society of Chemistry 2018

Open Access Article. Published on 23 April 2018. Downloaded on 2/20/2026 5:34:00 PM.
This article is licensed under a Creative Commons Attribution-NonCommercial 3.0 Unported Licence.

formed on the Rh surface during $CO_2$ hydrogenation over both alumina and silica supported catalysts suggesting that a metallic Rh phase is required for the dissociation of $CO_2$. However, the oxygen resulting from the $CO_2$ dissociation reacts with some other Rh atoms and form $RhO_x$ as revealed by XAS and XRD measurements. The linearly adsorbed CO species on metallic Rh are responsible for the higher activity of $Rh/Al_2O_3$. Thus, it is concluded that $CO_2$ methanation over $Rh/Al_2O_3$ proceeds by the dissociative adsorption of $CO_2$ giving rise to linearly adsorbed CO species on reduced Rh ($Rh–CO_{lin}$) while the adsorbed O can interact with other Rh atoms forming $RhO_x$.

## Conflicts of interest

There are no conflicts to declare.

## Acknowledgements

The authors would like to thank ESRF for providing the beamtime. Parts of this research were carried out at PETRA III at DESY, a member of the Helmholtz Association (HGF). P. Velin and E. C. Adams are acknowledged for their contribution to sample preparation. This work was financially supported by the Swedish Research Council through the Röntgen–Ångström collaboration "Time-resolved *in situ* methods for design of catalytic sites within sustainable chemistry" (No. 349-2013-567), the Swedish Foundation for Strategic Research through the project "Novel two-dimensional systems obtained on SiC as a template, for electronics, sensing and catalysis" (RMA15-0024), and the Competence Centre for Catalysis, which is financially supported by Chalmers University of Technology, the Swedish Energy Agency and the member companies: AB Volvo, ECAPS AB, Haldor Topsøe A/S, Volvo Car Corporation, Scania CV AB, and Wärtsilä Finland Oy.

## References

1 A. Shima, M. Sakurai, Y. Sone, M. Ohnishi and T. Abe, *Development of a $CO_2$ reduction catalyst for the Sabatier reaction, in 42nd International Conference on Environmental Systems 15-19*, San Diego, California, AIAA, July 2012, pp. 2012–3552.
2 G. A. Du, S. Lim, Y. H. Yang, C. Wang, L. Pfefferle and G. L. Haller, *J. Catal.*, 2007, **249**, 370–379.
3 M. Agneli, M. Kolb and C. Mirodatos, *J. Catal.*, 1994, **148**, 9–21.
4 M. Agneli, H. Swaan, C. Marquez-Alvarez, G. Martin and C. Mirodatos, *J. Catal.*, 1998, **175**, 117–128.
5 I. Fechete and J. C. Vedrine, *Molecules*, 2015, **20**, 5638–5666.
6 F. Solymosi and A. Erdöhelyi, *J. Mol. Catal.*, 1980, **8**, 471–474.
7 F. Solymosi, A. Erdöhelyi and T. Bansagi, *J. Catal.*, 1981, **68**, 371–382.
8 T. Iizuka, Y. Tanaka and K. Tanabe, *J. Mol. Catal.*, 1982, **17**, 381–389.
9 S. J. Tauster, S. C. Fung and R. L. Garten, *J. Am. Chem. Soc.*, 1978, **100**, 170–175.
10 A. R. Puigdollers, P. Schlexer, S. Tosoni and G. Pacchioni, *ACS Catal.*, 2017, **7**, 6493–6513.
11 M. N. Martin, P. Velin, M. Skoglundh, M. Bauer and P.-A. Carlsson, *Catal. Sci. Technol.*, 2017, **7**, 1086–1094.
12 P. Frontera, A. Macario, M. Ferraro and P. L. Antonucci, *Catalysis*, 2017, **7**, 59–87.
13 S. Rönsch, J. Schneider, S. Matthische, M. Schluter, M. Götz, J. Lefebvre, P. Prabhakaran and S. Bajohr, *Fuel*, 2016, **166**, 276–296.
14 S. Brunauer, P. H. Emmett and E. Teller, *J. Am. Chem. Soc.*, 1938, **60**, 309–319.
15 S. Pascarelli, *et al.*, *J. Synchrotron Radiat.*, 1999, **6**, 146–148.
16 E. C. Adams, M. Skoglundh, M. Folic, E. C. Bendixen, P. Gabrielsson and P.-A. Carlsson, *Appl. Catal., B*, 2015, **165**, 10–19.
17 B. Ravel and M. Newville, *J. Synchrotron Radiat.*, 2005, **12**, 537–541.
18 M. Newville, *J. Phys.: Conf. Ser.*, 2013, **430**, 012007–012014.
19 N. Schell, A. King, F. Beckmann, H.-U. Ruhnau, R. Kirchhof, R. Kiehn, M. Müller, A. Schreyer, R. Garrett and I. Gentle, *et al.*, The high energy materials science beamline (hems) at petra iii, *AIP Conf. Proc.*, 2010, **1234**(1), 391.
20 C. Zhang, J. Gustafson and L. R. Merte, *et al.*, *Rev. Sci. Instrum.*, 2015, **86**, 033112.
21 D. Bazin, D. Sayers, J. J. Rehr and C. Mottet, *J. Phys. Chem. B*, 1997, **101**, 5332–5336.
22 D. C. Bazin, D. A. Sayers and J. J. Rehr, *J. Phys. Chem. B*, 1997, **101**, 11040–11050.
23 A. Gayen, K. R. Priolkar, P. R. Sarode, V. Jayaram, M. S. Hegde, G. N. Subbanna and S. Emura, *Chem. Mater.*, 2004, **16**, 2317–2328.
24 S. Hosokawa, M. Taniguchi, Z. Utani, H. Kanai and S. Imamura, *Appl. Catal., A*, 2005, **289**, 115–120.
25 V. Marchionni, M. A. Newton, A. Kambolis, S. K. Matan, A. Weidenkaff and D. Ferri, *Catal. Today*, 2014, **229**, 80–87.
26 H. Hirata, K. Kishita, Y. Nagai, K. Dohmae, H. Shinjoh and S. Matsumoto, *Catal. Today*, 2011, **164**, 467–473.
27 C. P. Hwang, C. T. Yeh and Q. M. Zhu, *Catal. Today*, 1999, **51**, 93–101.
28 A. Karelovic and P. Ruiz, *Appl. Catal., B*, 2012, **113–114**, 237–249.
29 F. Solymosi and H. Knosinger, *J. Catal.*, 1990, **122**, 166–177.
30 M. A. Henderson and S. D. Worley, *J. Phys. Chem.*, 1985, **89**, 1417–1423.
31 W. H. Bragg and W. L. Bragg, *Proc. R. Soc. London, Ser. A*, 1913, **88**(605), 428–438.
32 https://icsd.fiz-karlsruhe.de (accessed January 2018).
33 I. A. Fisher and A. T. Bell, *J. Catal.*, 1996, **162**, 54–65.
34 H. Y. Luo, H. W. Zhou, L. W. Lin, D. B. Liang, C. Li, D. Fu and Q. Xin, *J. Catal.*, 1994, **145**, 232–234.
35 A. Karelovic and P. Ruiz, *J. Catal.*, 2013, **301**, 141–153.
36 A. Beuls, C. Swalus, M. Jacquemin, G. Heyen, A. Karelovic and P. Ruiz, *Appl. Catal., B*, 2012, **113–114**, 2–10.

Open Access Article. Published on 23 April 2018. Downloaded on 2/20/2026 5:34:00 PM.
This article is licensed under a Creative Commons Attribution-NonCommercial 3.0 Unported Licence.

37 S. S. C. Chuang, R. W. Stevens and R. Khatri, *Top. Catal.*, 2005, **32**, 225–232.
38 M. Jacquemin, A. Beuls and P. Ruiz, *Catal. Today*, 2010, **157**, 462–466.
39 D. I. Kondarides, P. Panagiotopoulou and X. E. Verykios, *J. Phys. Chem. C*, 2011, **115**, 1220–1230.
40 L. F. Liotta, G. A. Martin and G. Deganello, *J. Catal.*, 1996, **164**, 322–333.


This journal is © The Royal Society of Chemistry 2018